Cerebral Cortex December 2014;24:3365–3378
doi:10.1093/cercor/bht196
Advance Access publication August 7, 2013

Connectivity-Based Parcellation of the Human Temporal Pole Using Diffusion Tensor Imaging

Lingzhong Fan[1,2], Jiaojian Wang[3], Yu Zhang[1,2], Wei Han[4], Chunshui Yu[4] and Tianzi Jiang[1,2,3,5]

[1]Brainnetome Center, [2]National Laboratory of Pattern Recognition, Institute of Automation, Chinese Academy of Sciences, Beijing 100190, PR China, [3]Key Laboratory for NeuroInformation of Ministry of Education, School of Life Science and Technology, University of Electronic Science and Technology of China, Chengdu 625014, PR China, [4]Department of Radiology, Tianjin Medical University General Hospital, Tianjin 300052, PR China and [5]The Queensland Brain Institute, University of Queensland, Brisbane, QLD 4072, Australia

Lingzhong Fan and Jiaojian Wang equally contributed to this work.

Address correspondence to Tianzi Jiang, National Laboratory of Pattern Recognition, Institute of Automation, Chinese Academy of Sciences, Beijing 100190, PR China. Email: jiangtz@nlpr.ia.ac.cn

The temporal pole (TP) is an association cortex capable of multisensory integration and participates in various high-order cognitive functions. However, an accepted parcellation of the human TP and its connectivity patterns have not yet been well established. Here, we sought to present a scheme for the parcellation of human TP based on anatomical connectivity and to reveal its subregional connectivity patterns. Three distinct subregions with characteristic fiber pathways were identified, including the dorsal (TA*r*), the medial (TG*m*), and lateral (TG*l*) subregions, which are located ventrally. According to the connectivity patterns, a dorsal/ventral sensory segregation of auditory and visual processing and the medial TG*m* involved in the olfactory processing were observed. Combined with the complementary resting-state functional connectivity analysis, the connections of the TG*m* with the orbitofrontal cortex and other emotion-related areas, the TG*l* connections with the MPFC and major default mode network regions, and the TA*r* connections with the perisylvian language areas were observed. To the best of our knowledge, the present study represents the first attempt to parcel the human TP based on its anatomical connectivity features, which may help to improve our understanding of its connectional anatomy and to extend the available knowledge in TP-related clinical research.

Keywords: connectivity, diffusion tensor imaging, parcellation, resting-state fMRI, temporal pole

Introduction

Covering the anterior portion of the human temporal lobe (TP), the TP not only has been regarded as a structural uniform area in earlier brain atlases (Brodmann 1909; Economo and Koskinas 1925), but also has been proposed as a functional homogeneous region in previous literatures (Patterson et al. 2007; Simmons et al. 2010). Because little is known regarding human TP connectivity and function, it has been referred to as "the enigmatic TP" (Olson et al. 2007). However, anatomical tracer studies in nonhuman primates have revealed its rich connections in both cortical and subcortical structures, although such studies were usually confined to specific areas (Markowitsch et al. 1985; Moran et al. 1987; Kondo et al. 2003). Furthermore, numerous animal experiments as well as clinical and neuroimaging studies have demonstrated that the TP is an association cortex that not only is involved in multimodal sensory integration (Kondo et al. 2003; Poremba et al. 2003; Olson et al. 2007; Skipper et al. 2011; Visser et al. 2012), but also has been implicated in various high-order cognitive functions, including memory (Schacter and Wagner 1999; Munoz-Lopez et al. 2010), name and face recognition (Olson et al. 2007), emotion (Royet et al. 2000), empathic behavior (Rankin et al. 2006), social cognition (Zahn et al. 2007, 2009; Green et al. 2010; Olson et al. 2012), and higher-order aspects of language, such as sentence processing (Hickok and Poeppel 2007) and semantic memory (Binney et al. 2010). The diversity of its functions and connections suggests the presence of subregions within this area and their participation in different functional networks.

However, there has been much debate regarding how the TP should be partitioned on the basis of various criteria from observer-dependent histological studies. Although it has been previously described as a uniform area in earlier cytoarchitectonic or myeloarchitectonic atlases (see Supplementary Fig. 1*A*,*B*), different views on TP parcellation also exist. According to fiber myelogenesis, Flechsig (1920) differentiated the anterior polar region with its dorsal part as Feld 13, its medial part as Feld 13b, and its ventral part as Feld 18b in his myelogenetic map (see Supplementary Fig. 1*C*). Moreover, one myeloarchitectonic parcellation study demonstrated 5 subregions in this area (Hopf 1954). Furthermore, 2 recent postmortem studies using different histological criteria found that the TP could be separated into different cytoarchitectonic subfields (Ding et al. 2009; Blaizot et al. 2010). Although potential explanations for inconsistent TP parcellation may be the variable extents of the human TP and the different methodologies used and their inherent limitations, because of the lack of an accepted description of the TP subregions, further understanding of TP function in vivo has been overlooked and even disputed in relevant studies. Moreover, given that TP dysfunction has also been associated with multiple neurological disorders, including schizophrenia (Gur et al. 2000; Crespo-Facorro et al. 2004), semantic dementia (Olson et al. 2007; Patterson et al. 2007), epilepsy (Semah 2002; Chabardes et al. 2005), Alzheimer's disease, and Pick's disease (Arnold et al. 1994), an established parcellation frame with a systematic connectivity analysis for the human TP in vivo would be helpful for further understanding the malfunctions induced by such diseases.

Previous studies have suggested that the functional and/or structural heterogeneity of a brain region correlates with its connectivity pattern; thus, the patterns of its anatomical connectivity reflect the segregation of distinct areas (Passingham et al. 2002; Averbeck et al. 2009; Eickhoff et al. 2010; Caspers

et al. 2011). Using noninvasive diffusion tensor imaging (DTI) with fiber tractography, researchers can successfully define brain regions or subregions based on distinct connectivity patterns in vivo, which have proven to be highly consistent with traditional cytoarchitectonic findings (Behrens, Johansen-Berg, et al. 2003; Johansen-Berg et al. 2004; Beckmann et al. 2009; Bach et al. 2010; Mars, Jbabdi, et al. 2011; Cloutman and Lambon Ralph 2012; Wang, Fan, et al. 2012). Therefore, by adopting such a parcellation strategy, we could separate the subdivisions in the human TP. In addition, due to the numerous anatomical connections to and from the TP, its functions may be connected with a more extensive and complex network, rather than involving only the TP itself. Currently, most knowledge regarding TP connectivity in the human brain has been based on cross-species generalizations, which may not precisely correspond to that in humans owing to morphological differences and evolution (Gloor 1997). Thus, it is necessary to identify human TP connections in vivo, particularly the more comprehensive structural and functional connectivity patterns at the subregional level. Binney et al. (2012) revealed the connectivity patterns of morphologically defined subregions in the rostral temporal lobe using diffusion imaging probabilistic tractography. However, this study mainly focused on the cortico-cortical connections of the rostral temporal lobe with the intratemporal and extratemporal cortices that were confined to the frontal and parietal language areas.

In the current study, first we parceled the human TP into 3 subregions based on its anatomical connectivity features. Then, using subsequent probabilistic fiber tracking and resting-state functional connectivity (RSFC) analysis, we sought to clarify the anatomical and functional connectivity patterns of each subregion. This present study extends upon the earlier connectivity study in 2 ways: (1) Connectivity to the nontemporal lobe regions is covered in more detail, including both the cortical and subcortical structures, and (2) RSFC analysis was employed to determine the potential functional systems in which they participate.

Materials and Methods

Participants and Data Acquisition

Two independent groups of healthy subjects were recruited via advertisement for diffusion magnetic resonance imaging (MRI) and resting-state functional MRI (fMRI) data acquirement. All of the subjects were right-handed as assessed by the Edinburgh handedness inventory and were free of any psychiatric or neurological abnormalities. Informed consent was obtained from all subjects as approved by the local medical ethics committee. All of the acquired datasets were visually inspected by 2 experienced radiologists (W.H. and CS.Y.) for apparent artifacts and distortions arising from subject motion and instrument malfunction. Data with an apparent signal loss and distortions in the TP regions were excluded to ensure adequate signal coverage in the relevant regions for subsequent analysis.

First, we acquired diffusion-weighted echo-planar images (using the following parameters: Repetition time (TR) = 15 000 ms, echo time (TE) = 73 ms; 69 contiguous axial slices with an isotropic 2-mm resolution, matrix size = 128 × 128) in 18 healthy, right-handed participants (9 males; age range = 22–30 years, mean age = 25.9, standard deviation = 2.3) using a GE 3.0-T Signa HDxt scanner (General Electric, Milwaukee, USA) with an 8-channel phased-array head coil. Diffusion weighting was distributed along 50 directions using a *b*-value of 1000. For each set of diffusion-weighted data, 3 volumes with no diffusion weighting were acquired at points throughout the acquisition. In addition, for volumetric and registration purposes, a set of high-resolution T_1-weighted images were acquired sagittally using a fast inversion-recovery-prepared 3-dimensional (3D) gradient-echo sequence (without interslice gap, TR = 7.79 ms, TE = 2.98 ms, flip angle = 7°, matrix size: 256 × 256; field-of-view (FOV): 256 × 256 mm^2; slices: 188 in sagittal orientation).

Secondly, the resting-state fMRI data and related T_1-weighted images were collected from a different group of 18 healthy, right-handed volunteers (9 males; age range = 21–31 years, mean age = 26.2, standard deviation = 2.1) using a 3.0-T Siemens MRI scanner. An fMRI was performed during the resting state, and the subjects were instructed to rest with their eyes closed, relax their minds, and remain as motionless as possible during the echo-planar imaging (EPI) data acquisition. Echo-planar images (180 volumes) were acquired using a gradient-echo, single-shot, EPI sequence (TR = 2000 ms, TE = 30 ms, flip angle = 90°). The slice thickness was set to 3 mm (slice gap = 0.9 mm) with a matrix size of 64 × 64 and an FOV of 220 × 220 mm^2, which resulted in a voxel size of 3.4 × 3.4 × 3.9 mm^3. A structural scan was also acquired for each participant in the same session, using a T_1-weighted 3D magnetization-prepared rapid gradient-echo (MP-RAGE) sequence (TR/TE = 2000/2.2 ms; flip angle = 9°) with a voxel size of 1 × 1 × 1 mm^3.

Data Preprocessing

The diffusion and structural MR data were preprocessed using the FMRIB's Diffusion Toolbox (FMRIB Software Library, FSL, 4.0; http://www.fmrib.ox.ac.uk/fsl) and the MINC Toolbox (http://www.bic.mni.mcgill.ca/ServicesSoftware/MINC). First, brain extraction was performed on the nondiffusion-weighted images ($b = 0$ s/mm^2) using the brain extraction tool (BET) in FSL (Smith 2002). Secondly, after being converted into the MINC format, the structural MR images were corrected for nonuniformity artifacts using the nonparametric nonuniform intensity normalization (N3) algorithm to improve the accuracy of the following anatomical analysis (Sled et al. 1998). Next, the skull-stripped T_1-weighted images of each subject were linearly transformed into the previously processed nondiffusion *b*0 images using the registration program (minctracc) available with MINC tools, which provided a set of coregistered T_1 images in a native DTI space. Subsequently, the coregistered T_1-weighted images in the diffusion space were first registered to the Montreal Neurological Institute (MNI) template using linear (lsq9, i.e. 3 rotations, 3 translations, and 3 scales) transformations. Next, the linear transformed T_1-weighted images were nonlinearly warped into the MNI template (Collins et al. 1994). Finally, the derived transformation parameters were then inverted and used to warp the seed and target masks from the MNI space to the native DTI space using nearest-neighbor interpolation.

Definition of TP Boundary

In general, the TP is anteriorly bordered by the hemispheric margin and posteriorly bordered by a coronal plane before the limen insulae (or frontal–temporal continuity). Within the MNI152 brain template, we defined the TP boundary as following a rostrocaudal sequence (see Supplementary Fig. 2) and considered the description of the segmentation criteria previously reported by Insausti et al. (1998). First, the appearance of the collateral sulcus confirmed the end of the TP ventral-medially, which also marked the beginning of the entorhinal and perirhinal cortices. Secondly, the rostral-most extension of the superior temporal and inferior temporal sulci provided an approximation for the dorsal and lateral limits of the TP. Moreover, according to the description provided by Insausti et al., the polar sulci were the major anatomical landmarks between the TP and superior temporal gyrus (STG). However, there are usually mismatches between the sulci anatomy and the cytoarchitecturic results, particularly for the dorsolateral boundary of the TP. Thus, the dorsal boundary between the TP and STG (Brodmann area 22, BA22) was not defined, and parts of the STG may be included in the TP seed mask. In addition, according to the rostral-most extension of the superior temporal and inferior temporal sulci, the middle temporal gyrus (MTG; BA21) was removed from the TP seed mask. Finally, compared with Brodmann's atlas, which was available on the Caret5 software (Van Essen et al. 2012), a macroscopically defined TP seed mask in our study approximately resembled BA38 (Fig. 1). Next, the bilateral TP seed masks were warped back to

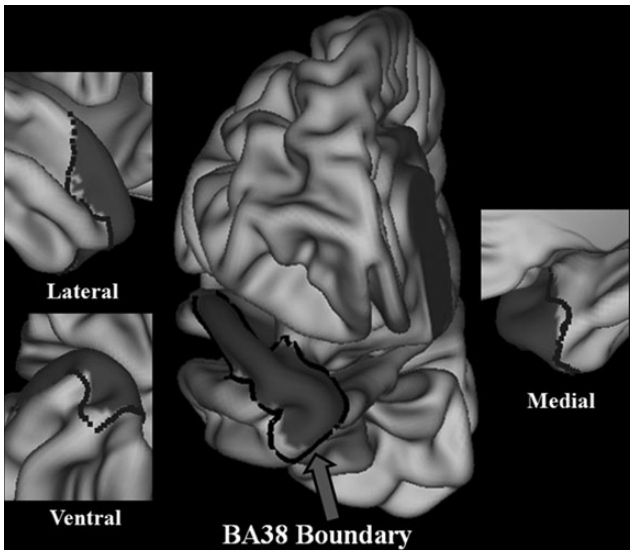

Figure 1. Views of the frontal, ventral, medial, and lateral aspects of the human brain show the location of the TP. The TP is defined on the MNI152 brain template with a black line indicating the boundary of BA38 from the Brodmann surface atlas in the Caret5 software. The left TP was shown as an example for boundary definition and superimposed on the surface template.

the individual native DTI space using the inverse of the linear transformation and nonlinear deformations. Subsequently, the final TP seed masks were confirmed on the coronal planes, slice-by-slice, to include all tissue commonly assigned to the TP cortex.

Connectivity-Based Parcellation of TP

Analysis of the diffusion-weighted images was performed using the FSL software package. First, the diffusion-weighted images were realigned to the nondiffusion *b*0 images using an affine transformation for the correction of head motion and eddy current-induced image distortion. Next, the probability distribution was estimated on multiple fiber directions at each voxel in the diffusion data. The vectors in the anterior temporal regions were displayed using lines to represent the principle diffusion direction at each voxel using red, green and blue coding in 4 example subjects (see Supplementary Fig. 3). These vector maps showed that there were sufficient signals with little distortion in the TP region. Signal dropout and stacking in the ventral region behind the pole were observed, although mainly located in the gray matter, which would still affect white matter (WM) and place limitations on the observed connectivity results in this area (Embleton et al. 2010). Next, to estimate the connectivity probability, probabilistic tractography was applied by sampling 5000 streamline fibers per voxel. The connectivity probability from the seed voxel i to another voxel j was defined by the number of fibers passing through voxel j divided by the total number of fibers sampled from voxel i (Behrens, Woolrich, et al. 2003; Behrens et al. 2007). Finally, the connections were estimated between voxels in the TP and all of the remaining voxels in the brain and stored at a lower resolution with a voxel size of $5 \times 5 \times 5$ mm (Johansen-Berg et al. 2004). Based on the native connectivity matrix, a cross-correlation matrix was calculated to quantify the similarity/dissimilarity between the connectivity profiles of the TP seed voxels. The cross-correlation matrix was also processed using spectral clustering (Ng et al. 2002), which is a method that groups data on the basis of its similarity to other data; the more similar their connectivity profiles, the more likely the voxels will be grouped together.

For clustering, no spatial constraint was applied when identifying the clusters. In addition, the grouping of voxels was entirely dependent on the anatomical connectivity information. Based on the following 2 considerations, the spatial constraint was not employed in the clustering step. First, the spectral clustering algorithm makes use of the eigenvectors of the similarity matrix as a feature for clustering, which was less sensitive to the spatial distance effects compared with other general clustering methods, such as the *k*-means algorithm. Secondly, how to balance the connectivity information and spatial distance information in the clustering when the spatial constraint was included is still an unresolved issue. According to previous studies (Tomassini et al. 2007; Mars, Sallet, et al. 2011), we also applied the spatial distance to correct the parcellation results for 2 example subjects. We found that when the distance effects were included (for the adjustor factor: from 0.1 to 1.0 with 0.1 as the interval), the parcellation results had clearly not improved, and the spatial constraint had changed boundaries between each pair of TP subregions (see Supplementary Fig. 4). In addition, the subregions in the TP cortex were observed to be spatially contiguous, although a few discontinuous voxels were shown in the individual parcellation results, which may be caused by noise or preprocessing steps. Finally, to visualize the TP parcellation results, we created maximum probability maps (MPMs) for each TP subregion, which were effective in decreasing the relatively discontinuous voxels with low probabilities.

In addition, to avoid an arbitrary choice in the number of clusters, we used cross-validations to determine the number of clusters, which yielded optimal consistency across subjects and thus, an optimal number of clusters. Specifically, we employed the leave-one-out method where the data from each subject were excluded from averaging. For each subject, we verified the consistency between the clustering results of the single subject and the average across the remaining subjects using Cramer's V. Cramer's V has values in the interval [0, 1], where high values indicate good consistency. A value of "1" indicated a perfect match. The intersubject consistency check was also performed for $k = 2, 3, 4, 5$ clusters.

Moreover, the population probability maps of the resulting clusters were derived from the overlapping of these clusters (in standard brain space) across subjects and divided by the number of subjects, so that the voxel values in the population probability maps represented the proportion of the population in which a cluster was present. In addition, we created the MPMs in the standard (MNI) space for each TP subregion, which retained quantitative information regarding the intersubject variability. We adopted the Ding et al. (2009) nomenclature to label the observed TP subregions.

Mapping Anatomical Connectivity Patterns

First, to determine the major differences in connection patterns that drive this connectivity-based parcellation, we used the TG*m*, TG*l*, and TA*r* regions (thresholded at 50% probability) as seeds for probabilistic tractography using estimates of the (multiple) fiber orientations in each voxel (Behrens et al. 2007). The connection probability between a seed and another voxel in the brain is given by the number of traces arriving at the target site. Furthermore, an individual-level threshold for the probabilistic fiber tracking combined with a group-level threshold for the fiber tracking success rate across all subjects was used (Kucyi et al. 2012). At the individual level, we used a conservative threshold of the connectivity probability value $P \geq 2.0$ (i.e. ≥0.04% of the 5000 samples from the seed reaching target) to remove voxels with a very low connectivity probability. Next, at the group level, we maintained the consistently identified fibers and target brain areas across subjects with a success rate of ≥50%.

To reduce the number of false positives in fiber tracking, the raw tracts of each subject were first thresholded with a connectivity probability value $P \geq 2.0$, that is, ≥0.04% of the 5000 samples generated from each seed voxel. The fiber tracts were then binarized and warped into the standard MNI space according to the corresponding estimated transformations. We subsequently averaged the warped fiber tracts across subjects to obtain population maps, which were then thresholded to display only those voxels that were present in at least 50% of the subjects. In addition, we used the Johns Hopkins University (JHU) WM tractography atlas to label the fiber pathways (Wakana et al. 2004).

Secondly, we employed the automated anatomical labeling (AAL) atlas (Tzourio-Mazoyer et al. 2002) to subdivide the cerebral cortex and subcortical nuclei of each subject into different target areas (43 areas for each hemisphere with the TP and cerebellum excluded). In

addition, we further replaced the thalamus in the AAL atlas with a finer-grained thalamic atlas (Behrens, Johansen-Berg, et al. 2003), so that 49 target brain areas were completely acquired for each hemisphere. Next, for each subject, we drew 5000 samples from the connectivity distribution (starting from the seed voxels in the TP subregions) and computed the average probability of connection for each seed–target combination. A connection probability value was then normalized and averaged for each seed–target combination across all the subjects. Finally, we selected those target brain areas that met both the individual- and group-level criteria in both hemispheres simultaneously to estimate the anatomical connectivity fingerprints.

Finally, to test for the effect of within-subject factors on the "TP subregions" (TG*m*, TG*l*, and TA*r*), "target areas" and "hemispheres" (left and right), as well as on the interactions of the TP subregions with the selected 17 target brain areas in each hemisphere, we performed repeated-measures analysis of variance (ANOVA) on these connection probability values. The Huyhn-Feldt adjustment was used when necessary. Next, multivariate analysis of variance with subsequent univariate ANOVAs and Bonferroni pair-wise comparisons were performed to identify the specific differences between each pair of TP subregional connection probabilities with ipsilateral target areas. These statistical analyses were performed using SPSS 18.0 (IBM, Armonk, NY, USA).

Resting-State fMRI Connectivity Analysis of the TP Subregions

Preprocessing of the resting-state fMRI data was performed using the scripts provided by the 1000 Functional Connectomes Project (www.nitrc.org/projects/fcon_1000) (Biswal et al. 2010) with both the FSL (http://www.fmrib.ox.ac.uk/fsl/) and AFNI (Automated Functional NeuroImaging) (http://afni.nimh.nih.gov/afni) software. The preprocessing steps consisted of (1) discarding the first 10 volumes in each scan series to allow for signal equilibration, (2) performing slice-timing correction, (3) performing motion correction, (4) time series despiking, (5) spatial smoothing with a 6-mm full-width at half-maximum Gaussian kernel, (6) normalizing the mean-based intensity, (7) band-pass temporal filtering (0.01 Hz < f < 0.10 Hz), (8) removing linear and quadratic trends, (9) performing linear and nonlinear spatial normalization of the structural MR images to the MNI152 brain template (MNI152, and conducting other anatomical data preprocessing steps; including brain masking and tissue classification), (10) coregistering the anatomical volume with the mean functional volume, (11) performing nuisance signal regression (WM, cerebrospinal fluid, the global signal, and 6 motion parameters), and (12) resampling the functional data into the MNI space with the concatenated transformations. Finally, 4-dimensional (4D) residual time series data in the standard MNI space for each subject were acquired after the preprocessing. No participant had a head motion of >1.5 mm maximum translations in the x, y, and z directions or 1.5° in any angular rotation.

In addition to visual inspection of the original data, to provide evidence for sufficient signal coverage in the TP, a leave-one-subject-out strategy, in which a single subject is iteratively excluded, was performed to analyze the intersubject stability of the connectivity patterns. To achieve this, we first averaged the connectivity matrices for the $N-1$ subjects and then computed the correlation between the averaged connectivity pattern and the connectivity pattern of the left-out subject for each TP voxel. Finally, the correlation matrices were then averaged across all steps to obtain the average stability map (Kahnt et al. 2012). Moreover, the temporal signal-to-noise ratio (TSNR, the ratio of the average signal intensity to the signal standard deviation) maps were calculated for each subject. Then, the individual TSNR maps were normalized into the standard MNI space and averaged. The averaged TSNR map showing signal coverage over the anterior temporal lobes could be found in Supplementary data (see Supplementary Fig. 5). As demonstrated by measurements of the TSNR, signal quality in the anterior temporal lobe was acceptable for RSFC analysis (Murphy et al. 2007).

Using the 4D residual time series data acquired in the processing step, we extracted the time course and averaged across all voxels for each functional region of interest (ROI) in the TP subregions. These ROIs consisted of spheres with a radius of 6 mm constructed around the center of each TP subregion by MRICron (http://www.sph.sc.edu/comd/rorden/MRicron/). For each individual dataset, the functional connectivity between the ROI time series and that of each voxel in the rest of the brain was represented by Pearson's correlation coefficient. To reduce the computational complexity, correlations were computed only between the gray matter voxels. Correlation coefficients were then normalized using Fisher's z-transform.

A 1-sample t-test ($n = 18$ subjects) on these maps was performed to test for areas where the averaged normalized correlation was significantly different from 0. Moreover, paired t-tests were used to identify the precise regions between each pair of TP subregions ipsilaterally that differed in their RSFC strengths. For the above voxel-wise comparisons, the false discovery rate (FDR) method was used for multiple comparison correction ($P < 0.01$), and only clusters containing a minimum of 50 voxels were reported here.

Results

Connectivity-Based Parcellation of the TP into 3 Subregions

Using probabilistic tractography of in vivo DTI data and clustering algorithms, 3 distinct subregions with various connectivity patterns were identified in an individual space for each subject. These results were transformed and combined in a standard MNI brain space to create a probabilistic, population-based parcellation of the TP including the dorsal TP (TA*r*), medial TP (TG*m*), and lateral TP (TG*l*), and the last 2 subregions located in the ventral part of the TP. The maximum probabilistic maps (Fig. 2*A*) and probabilistic maps of the TP subregions were calculated across 18 subjects and are shown in the lower row of Figure 2*B*. In addition, to determine the reliability of the spectral clustering method in selecting the optimal number of subregions, a consistent method was employed to verify the number with $K = 2$–5. With $K = 2$ and 3, the stability of the clustering was higher (Fig. 3).

Anatomical Connectivity Patterns of the TP Subregions

Statistical Analysis of the Connection Probabilities

Repeated-measures ANOVA demonstrated a significant main effect of the factor TP subregions ($F = 72.14$; $P < 0.0005$), indicating that the mean connection probabilities of the connections to all targets differed significantly among the 3 TP subregions. In addition, we also revealed a significant interaction ($F = 166.86$; $P < 0.0005$) between the TP subregions and target areas, revealing that the distribution of the connection probabilities to an individual target area was different among the TP subregions. Using MANOVAs, there were also statistically significant differences among the TP subregions in their anatomical connections in both hemispheres (left: $F = 67.56$, $P < 0.0005$ and right: $F = 75.87$, $P < 0.0005$). The detailed commonalities and differences in the TP subregional connectivity patterns acquired by the subsequent univariate ANOVAs and Bonferroni pair-wise comparisons are presented in Table 1. In addition, no significant main effect of the factor target areas was observed ($F = 0.00$; $P = 1.00$), and a significant interaction between TP subregions with hemisphere ($F = 5.20$; $P = 0.007$) was observed, indicating the asymmetric anatomical connectivity of the TP subregions.

Differences in Anatomical Connectivity Among the TP Subregions

First, using the JHU WM atlas, several major fibers were distinguished, including the uncinate fasciculus (UF), inferior

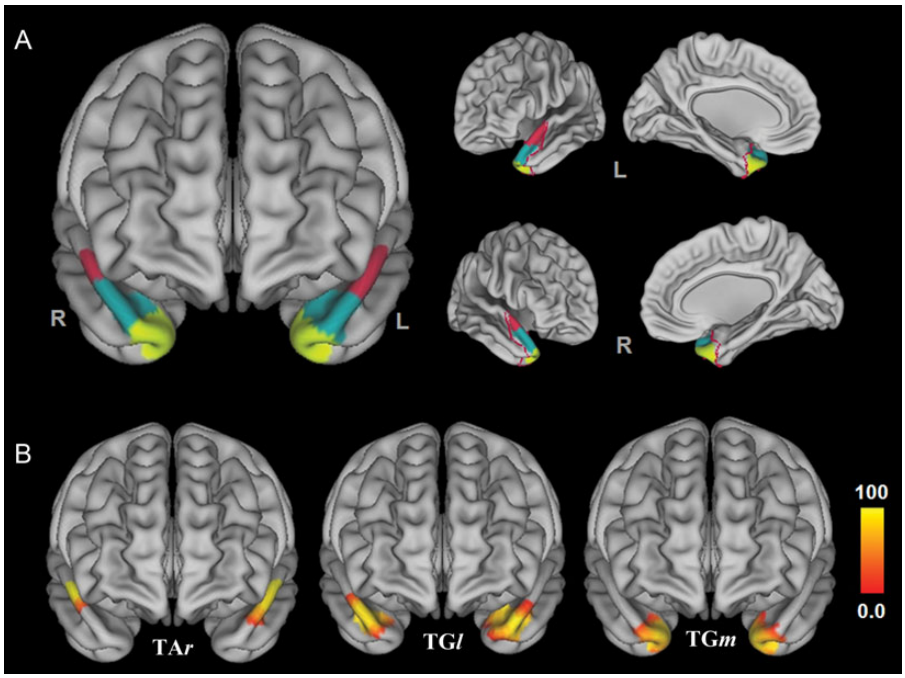

Figure 2. Connectivity-based parcellation of the TP into 3 subregions. The maximum probabilistic maps of the TP subregions [TG*m* refers to the medial TP (yellow); TG*l* refers to the lateral TP (green), and TA*r* refers to the dorsal TP (red)] were presented in Figure 1*A*. Figure 1*B* showed the probabilities for each voxel in each TP cortex to be classified into 1 of the 3 clusters. The color scheme represented the probability of the overlapping brains in each voxel across all the subjects. The maps are projected onto a 3D brain surface using the Caret5 software.

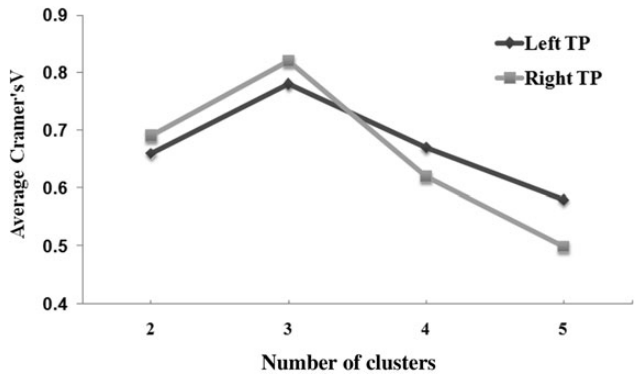

Figure 3. Average Cramer's V as an indication of clustering consistency. Cramer's V has values in the interval [0, 1] in which high values indicate good consistency. A value of "1" indicates a perfect match. Cramer's V was significantly higher for the 2 and 3 cluster solutions.

longitudinal fasciculus (ILF), middle longitudinal fascicle (MdLF), inferior fronto-occipital fasciculus (IFOF), and inferior thalamic peduncle (ITP; see Fig. 4 and Supplementary Fig. 7). Furthermore, the underlying fibers between the TP subregions with the thalamus could also be categorized into 2 main paths as previously described in the previous study (Behrens, Johansen-Berg, et al. 2003). One path traveled around the posterior edge of the thalamus and extended through the hippocampus (HIP), and the other path extended along the medial wall of the thalamus and turned laterally to the amygdala (AMG). Secondly, the anatomical connectivity fingerprints between each TP subregion with the predefined target brain areas in the ipsilateral hemisphere were acquired (Fig. 5*A*,*C*) and showed obvious differences.

There were a total of 17 target brain areas (Fig. 5) meeting the criteria in each hemisphere, including the superior frontal gyrus-orbital cortex (ORBsup), inferior frontal gyrus-orbital cortex (ORBinf), olfactory cortex (OLF), gyrus rectus (REC), insular (INS), parahippocampal gyrus (PHG), lingual gyrus (LING), fusiform gyrus (FFG), STG, MTG, inferior temporal gyrus (ITG), AMG, HIP, and putamen (PUT). Moreover, 3 thalamic subregions from the connectivity-based thalamic atlas also met the criteria for estimating the anatomical connectivity fingerprints, including (1) the prefrontal-connected thalamus (THA.P), which corresponded to the anterior nuclear group, medial nuclear group, and ventral anterior nuclei; (2) the temporal-connected thalamus (THA.T), which corresponded to the pulvinar; and (3) the occipital-connected thalamus (THA.O), which corresponded to the lateral geniculate body and pulvinar. Furthermore, most of the target brain areas have been previously reported in nonhuman primate tract tracing studies (Pandya and Kuypers 1969; Aggleton et al. 1980; Markowitsch et al. 1985; Moran et al. 1987; Morecraft et al. 1992; Stefanacci et al. 1996; Lavenex and Amaral 2000; Saleem et al. 2000; Kondo et al. 2003; Munoz and Insausti 2005).

The diversities of the TP subregions within each target brain area are also shown in Figure 5*B*,*D*. Although several variations existed, similar anatomical connectivity patterns were observed in both hemispheres (Fig. 5 and Table 1). Among the 3 TP subregions in the left hemisphere, the ventrolateral TG*l* showed high connection probabilities with the superior frontal gyrus (orbital part), OLF, REC, INS, PUT (lenticular nucleus), THA.P, and THA.O. The ventromedial TG*m* showed strong connections with the PHG, ITG, FFG, HIP, AMG, and all the 3 thalamic subregions. For the dorsal TA*r*, stronger connections with the inferior frontal gyrus (orbital part), insular cortex, STG, and MTG were observed. Meanwhile, there were some

Table 1

Differences in the anatomical connections between each 2 TP subregions with target areas

TP subregion\target areas	ORBsup	ORBinf	OLF	REC	INS	HIP	PHG	AMYG	
Left									
F tests (*F*/*P*-value)	53.03/0.00*	51.74/0.00*	29.16/0.00*	27.24/0.00*	25.10/0.00*	83.97/0.00*	122.73/0.00*	54.43/0.00*	
TGl–TGm (*P*)	(+)0.00*	(+)0.00*	(+)0.00*	(+)0.00*	(+)0.00*	(−)0.00*	(−)0.00*	(−)0.00*	
TGl–TAr (*P*)	(+)0.00*	(−)0.00*	(+)0.00*	(+)0.00*	(+)0.00*	(+)0.01*	1.00	(+)0.00*	
TGm–TAr (*P*)	(+)0.04*	(−)0.00*	(+)0.00*	(+)0.00*	(−)0.00*	(+)0.00*	(+)0.00*	(+)0.00	
Right									
F tests (*F*/*P*-value)	47.37/0.00*	12.91/0.00*	65.23/0.00*	54.63/0.00*	218.34/0.00*	271.71/0.00*	265.89/0.00*	572.08/0.00*	
TGm–TGl (*P*)	(+)0.01*	(+)0.05*	(+)0.00*	(+)0.00*	(+)0.00*	(−)0.00*	(−)0.00*	(−)0.00*	
TGl–TAr (*P*)	(+)0.00*	(−)0.04*	(+)0.00*	(+)0.00*	(−)0.00*	(+)0.00*	0.78	(+)0.00*	
TGm–TAr (*P*)	(+)0.00*	(−)0.00*	(+)0.00*	(+)0.00*	(−)0.01*	(+)0.00*	(+)0.00*	(+)0.00*	
TP subregion\targets areas	LING	FFG	PUT	THA(O)	THA(P)	THA(T)	STG	MTG	ITG
Left									
F tests (*F*/*P*-value)	1.00/0.37	71.48/0.00*	9.14/0.00*	3.08/0.06	3.43/0.04*	36.94/0.00*	4452.65/0.00*	22.65/0.00*	69.09/0.00*
TGl–TGm (*P*)	1.00	(−)0.00*	(+)0.00*	1.00	0.61	(−)0.00*	0.33	0.16	(−)0.00*
TGl–TAr (*P*)	1.00	0.49	0.23	0.10	0.58	0.09	(−)0.00*	(−)0.00*	(+)0.00*
TGm–TAr (*P*)	0.50	(+)0.00*	(−)0.05*	0.13	(+)0.04*	(+)0.00*	(−)0.00*	(−)0.00*	(+)0.00*
Right									
F tests (*F*/*P*-value)	25.38/0.00*	180.94/0.00*	19.06/0.00*	125.76/0.00*	51.38/0.00*	649.89/0.00*	5343.09/0.00*	48.62/0.00*	22.43/0.00*
TGm–TGl (*P*)	(+)0.00*	(−)0.00*	(+)0.00*	(−)0.00*	0.23	(−)0.00*	(+)0.00*	(+)0.00*	(−)0.00*
TGl–TAr (*P*)	(+)0.00*	1.00	(+)0.00*	(+)0.00*	(+)0.00*	(+)0.00*	(−)0.00*	(−)0.04*	0.95
TGm–TAr (*P*)	0.51	(+)0.00*	0.35	(+)0.00*	(+)0.00*	(+)0.00*	(−)0.00*	(−)0.00*	(+)0.00*

Note: Using the univariate ANOVAs and pair-wise comparisons, differences in the TP subregions with each ipsilateral target brain areas, as well as the anatomical connections toward the different targets among the TP subregions, were reported here. The results were all adjusted for multiple comparisons with Bonferroni.

The "*" indicates that the mean difference was significant at the 0.05 level. The "+"and "−" indicate directions for the pair-wise comparison.

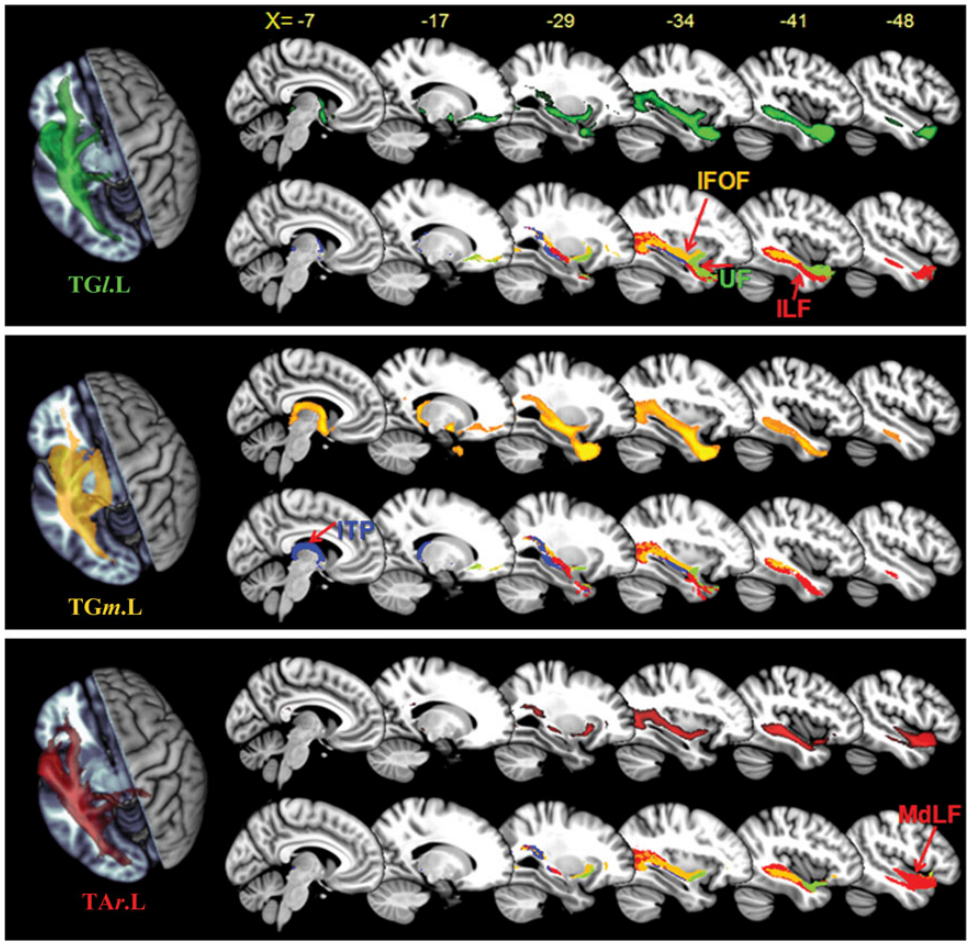

Figure 4. Population maps of the probabilistic tractography results from the left TG*m*, TG*l*, and TA*r* regions. Population maps of the probabilistic tractography results from the bilateral TP subregions are shown on the ICBM152 template in the MNI space with MRIcron. The color scales represent the population probability of a voxel belonging to a pathway for the TP subregions: TG*m* (warm), TG*l* (gray-green), and TA*r* (red-yellow). The main fiber tracts, including the UF, IFOF, MdLF, ILF, and ITPs were illustrated and marked.

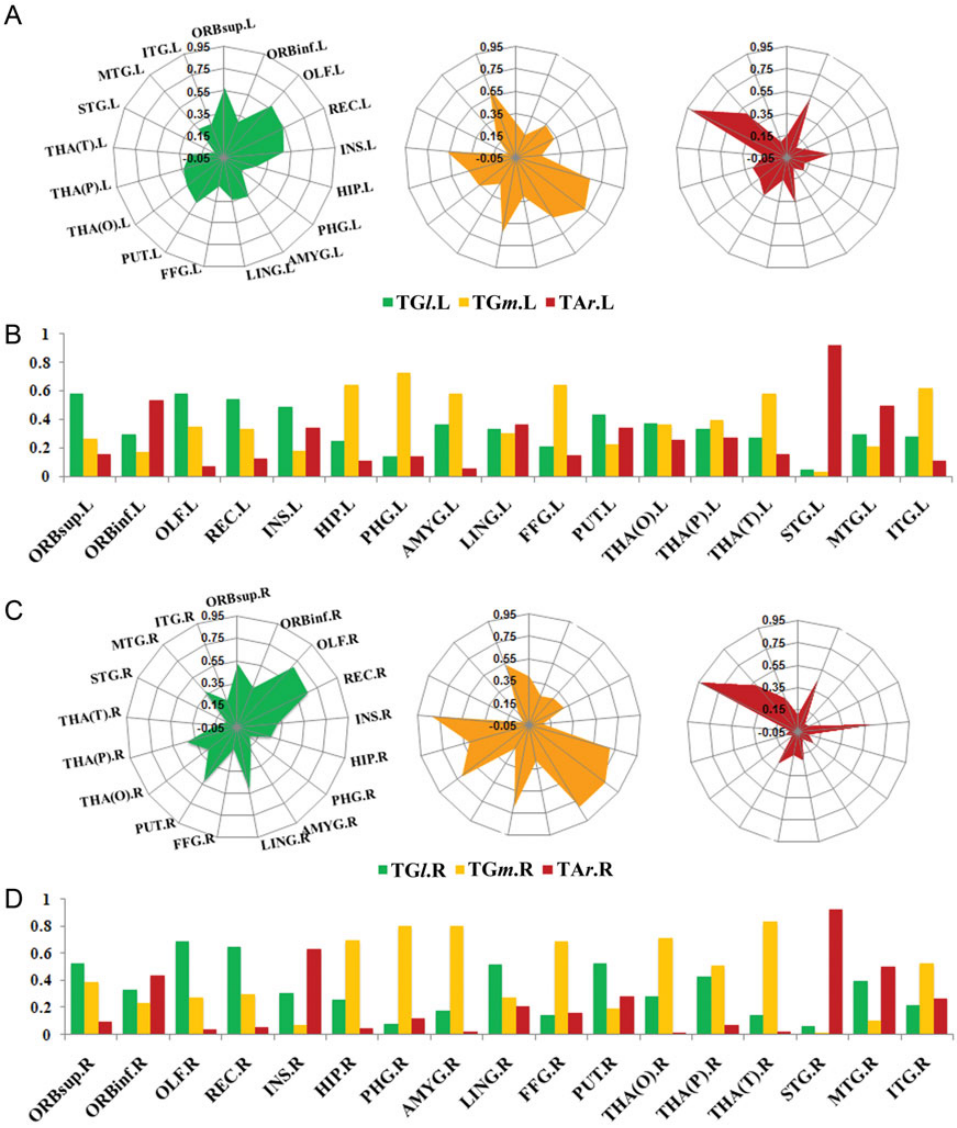

Figure 5. The anatomical connectivity fingerprints and quantitative differences of the bilateral TP subregional connections with target areas. Using the 17 brain target regions in the same hemisphere, the anatomical connectivity fingerprints were expressed via radar graphs in 6 individual maps (*A* for the left TP and *C* for the right TP). The quantitative results of the differences of the bilateral TP subregional connections with target areas are shown on the bar graphs (*B* and *D*).

differences in the right hemisphere. The right TG*l* showed stronger connections with the LING compared with the other 2 subregions, while no significant differences were observed in the left hemisphere. In addition, the right TA*r* showed weak connections with all the 3 thalamic subregions.

Functional Connectivity Patterns of TP Subregions

The average connectivity stability map is shown in Supplementary Figure 6 along with the distribution of the correlation coefficients. As shown in this stability map, the significant stability and the presence of similar connectivity profiles across different subjects demonstrated adequate signal coverage in the TP. In addition, the TSNR maps also showed sufficient signals in the anterior TP region (see Supplementary Fig. 5). Next, the RSFC patterns of each TP subregion were obtained. In addition, the bilateral TP subregions showed similar functional connectivity patterns for both the correlated and anticorrelated brain regions, as shown in Figure 6 and see Supplementary Figure 8. Disparate functional connectivity networks were systematically classified within the TP using RSFC with each subdivision, which suggested a discrete functional role. The RSFC results in the cerebellum are not shown in the figures.

Positively Correlated Networks

(1) The cortex in the TG*l* was positively correlated with the MTG, insular cortex, posterior temporoparietal junction (TPJ), and areas of the default mode network (DMN), including the medial prefrontal cortex (MPFC) and posterior cingulate gyrus. (2) The TG*m* was positively correlated with areas in the ventral MPFC, subcallosal gyrus, orbitofrontal cortex, and FFG. It was also correlated with areas in the medial temporal cortex, including the PHG, HIP, and AMG. (3) The dorsal TA*r* cortex was positively correlated with the STG, middle cingulate gyrus, supplement motor areas (SMA), anterior TPJ area, and perisylvian cortex, including the inferior frontal language areas and insular cortex.

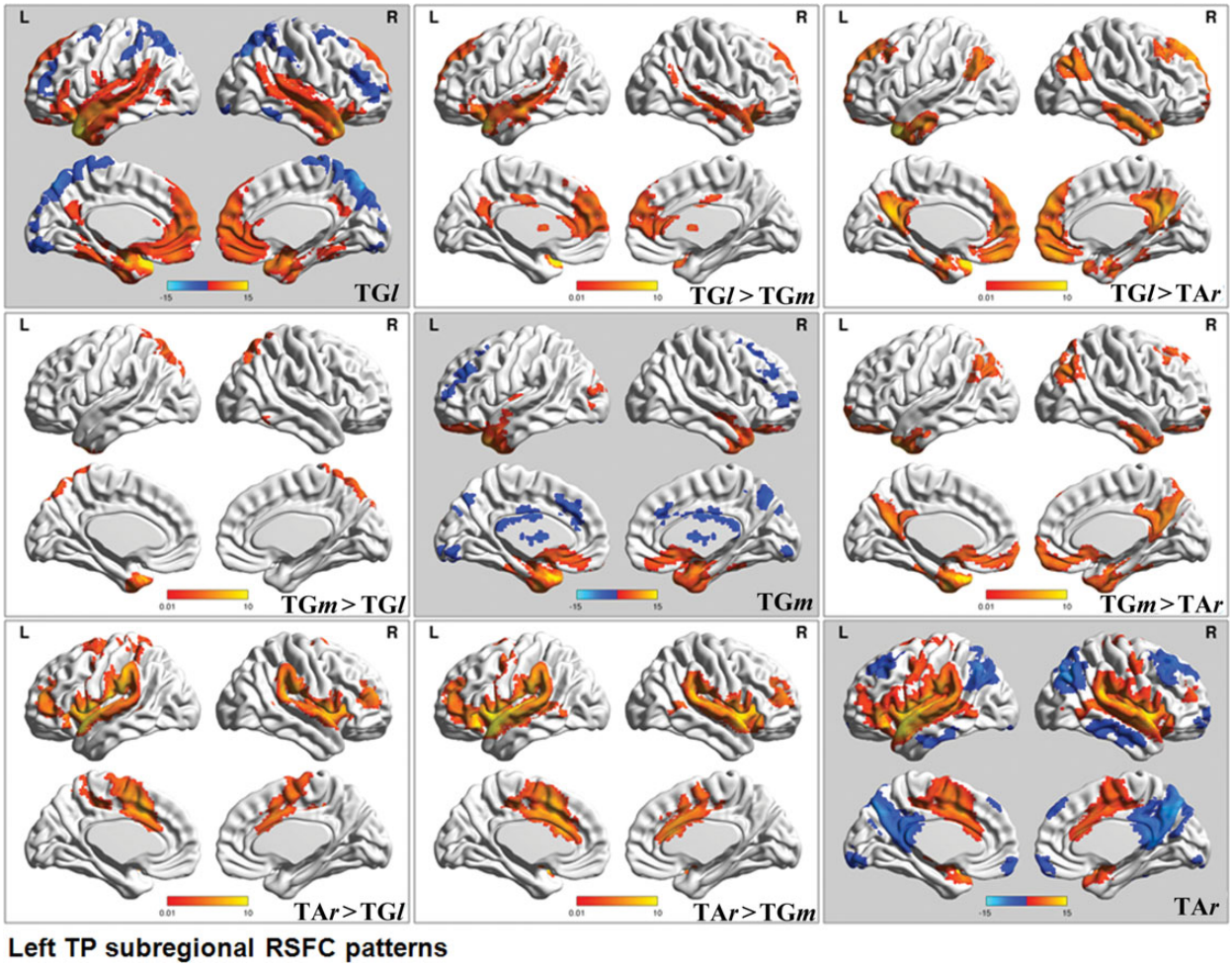

Figure 6. Spatial distribution of the RSFC patterns for the left TP subregions and the medial, lateral, and dorsal TP subregional RSFC variations. Statistical parametric maps are displayed using a voxel-level statistical threshold of $P < 0.05$ corrected for the FDR, with a cluster extent threshold of 50 voxels. The RSFC and relevancy connection differences maps are projected onto a 3D brain surface with intensity scales representing the *T*-values.

Anticorrelated Networks

(1) The TG*l* was negatively correlated with the bilateral dorsal prefrontal cortex, posterior parietal cortex, and dorsal precuneus. (2) The TG*m* was negatively correlated with the dorsal precuneus, part of the anterior cingulate gyrus, lateral middle frontal gyrus, and bilateral cerebellar Crus I/Crus II lobules and vermis regions. (3) The dorsal TA*r* was negatively correlated with the DMN areas, including the lateral inferior parietal lobule, posterior cingulate gyrus and precuneus, as well as the bilateral cerebellar Crus I and Crus II lobules. Thus, distinct anticorrelation patterns were observed between each of the TP subregions and different brain functional networks, which may reflect the competition between neuronal activities (Fox et al. 2005). Interestingly, reversed functional connections between the TP subregions and DMN areas were found. Specifically, the TG*l* showed positive correlations with the MPFC and precuneus, whereas the TA*r* showed negative connections with the precuneus.

The TP Subregional RSFC Variations

In addition, paired *t*-tests revealed significant connectivity differences between each pair of TP subregions. Compared with the TG*l*, the TG*m* showed a higher RSFC strength with the bilateral lateral orbital frontal cortex, posterior parietal cortex, and dorsal precuneus. In contrast, the TG*l* was identified with a stronger RSFC to the frontopolar, dorso-MPFC, and posterior cingulate cortex. When compared with the TA*r*, both the TG*m* and TG*l* showed higher connectivity with the classic DMN areas, including the posterior cingulate gyrus and precuneus, TPJ area, and MPFC. Moreover, the TG*l* showed higher connectivity in the dorso-MPFC, while the TG*m* showed more connectivity with the orbital cortex. In addition, the TA*r* showed higher connectivity with the SMA and perisylvian cortex compared with both the TG*m* and TG*l*.

Discussion

In the current study, we employed a data-driven approach to obtain a reliable subregional description of the human TP using connectivity-based parcellation with DTI. Three distinct subregions with characteristic connections were identified, including the dorsal (TA*r*), the medial (TG*m*), and lateral (TG*l*) subregions located in the ventral TP (Fig. 2). To confirm the suitability of our TP parcellation, we compared our results with existing histological parcellation findings and the multisensory organization of this area. Furthermore, the TP

subregional connections and their potential functional systems were also summarized. By mapping the fiber pathways (Fig. 4 and see Supplementary Fig. 7) and functional connectivity patterns (Fig. 6 and see Supplementary Fig. 8) in vivo, we observed a dorsal/ventral sensory segregation of the auditory and visual information processing in the TP and the medial TP associated with olfactory information processing. Moreover, combined with the complementary RSFC analysis, connections of the TG*m* with the orbitofrontal cortex and brain areas linked to emotion, the TG*l* connections with the MPFC and major regions of the DMN, and the TA*r* connections with the perisylvian language areas were observed.

Comparison with the Cytoarchitectonic/ Myeloarchitectonic Parcellations of the Human TP

Current connectivity-based parcellation of the human TP in vivo may be compared with those reported in cytoarchitectonic/myeloarchitectonic studies. First, the sum total of the 3 TP subregions corresponded approximately to BA38 (Fig. 1) and to area TG (Economo and Koskinas 1925), which indicated that the TP defined in these classic maps was not a homogenous cortical region, but contained several distinct areas. Secondly, compared with the Hopf temporopolar subregions (including the tp.l, tp.v, tp.d, tp.m, and tp/mt) based on the myeloarchitecture, it was shown that the TG*m* corresponded to Hopf area tp.m and TG*l* corresponded to the anterior part of area tp.d (Sewards 2011). Finally, consistent with 2 recently published histological works, the TG*m* and TG*l* in our study corresponded approximately to the temporopolar area TG in the description by Ding et al. (2009) and the area TPC (with medial and lateral subdivisions TPC*m* and TPC*l*) described in the study conducted by Blaizot et al. (2010). The dorsal TA*r* in our study also corresponded to part of the TA*r* area in the description by Ding et al., and an anterior part of area 22 described by Blaizot et al. However, care should be taken with these comparisons. Although the macroscopic defined TP seed in our study approximately resembles BA38, the defined extent of the TP was always variable in these studies. Secondly, the cytoarchitecture and connectivity architecture are 2 complementary anatomical properties of the brain and can influence each other. Although the cytoarchitecture may reflect the detailed inner organization of the cortical areas, the connectivity information is what actually determines the functions of the area (Passingham et al. 2002). However, the relationship between the 2 anatomical properties has not been well defined. A direct comparison of the in vivo parcellation results with the observer-dependent cytoarchitectonic or myeloarchitectonic findings should nevertheless be performed with caution.

Comparison with Sensory Segregation in the TP

The TP parcellation described in this study may be supported by studies reporting that the TP is a part of the association cortex involved in multimodal sensory integration. Both anatomical studies in the macaque and humans have suggested that there are sensory subdivisions in the TP. In the macaque, a sensory modality-specific organization was observed in the TP cortex with the dorsolateral parts of the TP receiving projections from the auditory association cortex, the ventral parts receiving projections from the extrastriate visual cortex, and the medial parts receiving projections from the prepiriform OLF (Kondo et al. 2003). Furthermore, cells in the dorsolateral and ventral TP were found to be sensitive to complex auditory and visual stimuli, respectively (Nakamura et al. 1994; Nakamura and Kubota 1996; Poremba et al. 2003). In terms of connectivity organization, the sensory parcellation in the macaque TP could provide supporting evidence for current human TP parcellation and subregional connectivity patterns. Furthermore, such sensory segregation was also presented in the human TP. Visser and Lambon Ralph (2011) found that the anterior superior temporal sulcus was activated in response to verbal and nonverbal sounds (but not pictures), whereas the basal region behind the TP was activated for all modalities and did not represent a purely visual area. Visser et al. (2012) show that the posterior ITG was preferentially responsive to pictures (over words), but that the anterior ITG was multimodal. The fusiform, however, remains preferentially sensitive to pictures. These functional data are consistent with the tracking data obtained from Binney et al. (2012) and in our study (details in the following Discussion section), which showed that the fusiform and PHG have the strongest connectivity to the TG*m* and explained the visual tendency of this region. In other fMRI studies, Skipper et al. (2011) found that the retrieval of semantic knowledge in the TP showed topographical differentiation based on the stimulus modality, that is, the human TP contains sensory subdivisions that fall along superior (auditory), inferior (visual), and polar (audiovisual) subdivisions. Consistent with this, the dorsal TA*r* and ventral TG*m* in our parcellation results may resemble the "superior" and "inferior" subdivisions described in the previous study. In addition, by reviewing neuroimaging studies that report the responses of human TP activations to a wide variety of tasks and stimuli, researchers found that the activations tended to follow a dorsal/ventral segregation based on whether the stimuli used were auditory or visual (Olson et al. 2007; Visser et al. 2010).

Human TP Subregional Connectivity Patterns and Putative Functions

*Dorsal TA*r

First, the TA*r* might participate in auditory processing via its connections to the association auditory cortex in the STG. Using probabilistic tractography with TA*r* as a seed, the main anterior part of the MdLF was observed. The MdLF courses within the WM of the STG rostrally to the primary auditory cortex, which could contribute to the auditory-verbal "what" pathway (Scott et al. 2000; Rauschecker and Scott 2009; Ueno et al. 2011; Binney et al. 2012). Moreover, it was reported that the most anterior part of the MdLF could terminate at BA38 (Makris et al. 2009; Wang, Fernandez-Miranda, et al. 2013). Secondly, compared with the other 2 TP subregions, stronger anatomical connections between the TA*r* with the orbital part of the inferior frontal gyrus (resembling BA47) were observed. This was consistent with the findings of Binney et al. (2012), which also found that the superior rostral temporal lobe showed the highest connection probability with BA47. Previous monkey studies indicated that there were association fibers via the UF that connected the most anterior part of the STG, that is, the anterior temporal lobes and dorsal part of the temporal polar proisocortex, with the lateral orbital frontal cortex (Petrides and Pandya 1988, 2002, 2009). Furthermore, the UF was considered a ventral limbic pathway that links the rostral STG, which is important for sound recognition (Clarke et al. 2002). In our subsequent RSFC

analysis, we demonstrated that the TA*r* was highly correlated with the inferior frontal language areas, which indicated that the bilateral TP was a critical region for language and might be confined to the TP dorsal parts (Pobric et al. 2007; Bi et al. 2010; Holland and Lambon Ralph 2010; Dewitt and Rauschecker 2012). Intriguingly, a previous monkey study also reported that there were significant neural activities in the dorsal TP that are sensitive to particular vocal calls of monkeys (Poremba et al. 2004). Thirdly, a higher anatomical connectivity probability (particularly in the right hemisphere) and stronger functional connectivity were also observed between the TA*r* and insular cortex. These connections between the TP and insular cortex were previously studied using axonal transport methods in the rhesus monkey (Mesulam and Mufson 1982) and DTI-based tractography in humans (Cloutman et al. 2012). The human TP combined with the orbitofrontal and insular cortices are recognized as components of the paralimbic loop, where multimodal integration occurs to modulate behaviors arising from the interactions between the internal and external environments (Mufson and Mesulam 1982). Based on the specialized TP subregional connectivity pattern, it appears likely that the TA*r* might be mainly involved in the paralimbic loop (Blaizot et al. 2010).

*Lateral TG*l

This subregion was located ventrolaterally in the TP. Based on its anatomical connections, the TG*l* was strongly connected with the orbital part of the superior frontal gyrus and REC. Furthermore, the TG*l* also showed significantly stronger connections with the MPFC compared with the other 2 TP subregions via RSFC analysis. Such connectivity patterns of the TG*l* with the orbital frontal cortex and MPFC were consistent with previous tract tracing studies (Kondo et al. 2003) and novel diffusion spectrum imaging findings in the monkey (Schmahmann et al. 2007). Using fiber tracking initiated from a seed in the TG*l*, which is the most rostral temporal lobe fiber bundle, the UF could be tracked, which links the rostral TP subregions with the ventral, medial, and orbital parts of the frontal lobe. Moreover, the TG*l* was also dominantly connected with other major DMN regions, which may indicate that the previously identified DMN subsystem (i.e. the lateral temporal cortex) could extend to the lateral TP (Buckner et al. 2008). However, evidence has shown the spatial and functional convergence of the DMN and semantic memory system (Binder et al. 2009; Wirth et al. 2011). Recently, Olson et al. (2012) reported that portions of the anterior temporal lobe played a critical role in representing and retrieving social knowledge, which is a specific type of semantic memory. According to the connectivity patterns, we assumed that the ventral lateral TG*l* may be involved in multimodal semantic processing (Visser et al. 2012) and functions as part of the "social brain" (Frith U and Frith C 2010). In addition, the underlying fiber tract, known as the ILF, could be tracked from the TG*l* seed, which was reported to play an important role in semantic processing and in linking object representations to their lexical labels (Mummery et al. 1999).

*Medial TG*m

Located ventromedially, the TG*m* may be involved in visual processing by integrating with the ventral and lateral temporal association visual cortices (Olson et al. 2007). Here, the ILF could also be tracked from the TG*m*, which was reported to carry visual information from the occipital areas to the temporal lobe (Catani et al. 2003). Furthermore, the TG*m* was anatomically and functionally connected with the medial temporal olfactory structures, which indicated that the TG*m* might participate in processing sensory information from smell and taste (Nakamura et al. 2000). According to the RSFC analyses, the TG*m* was also positively correlated with the ventral MPFC, orbitofrontal cortex, and subcallosal gyrus. These RSFC connections between the TG*m* and frontal cortex were consistent with previous tracer studies (Kondo et al. 2003). Furthermore, our in vivo fiber tracking results further confirmed that the UF served as an underlying pathway connecting the medial TG*m* to the orbitofrontal areas (Catani et al. 2002). Kondo et al. (2003) showed that there were 2 subcomponents of the UF with differential connectivity between different TP subregions to different frontal-limbic areas. Consistent with the tractography results obtained by Binney et al. (2012), the UF could be tracked from all TP subregions in our study, which might indicate that it is most likely not a singular bundle.

In addition, the distinct TP subregions also showed different subcortical connection patterns. First, the anatomical connectivity fingerprints showed stronger connections between the thalamus (THA.P, THA.T, and THA.O) and ventral TP subregions (TG*l* and TG*m*), while the TA*r* showed weak connections with the thalamus, particularly in the right hemisphere. These thalamic subregions could resample to the thalamic nuclei, including the pulvinar and medial thalamic nuclear groups, which were reported to send its connections to the TP in monkey studies (Markowitsch et al. 1985; Moran et al. 1987; Gower 1989). Similar findings in monkey studies revealed that the caudal medial portion of the medial pulvinar was the principal thalamic source of afferents to the temporopolar cortex (Markowitsch et al. 1985). Furthermore, fiber tractography results from the TG*m* and TG*l* confirmed that the major anatomical pathways between the thalamus and TP mainly traversed around the posterior edge and medial wall of the thalamus (Aggleton and Mishkin 1984; Behrens, Johansen-Berg, et al. 2003). Secondly, previous anatomical studies in the rhesus monkey found that there were 2-way connections between the AMG and TP region (Nauta 1961; Amaral and Price 1984). Moreover, in humans, the amygdalo-temporal fasciculus originating at the rostrolateral surface of AMG and deep in UF was observed to specifically connect to the TP (Klingler and Gloor 1960). Here, we observed that only the subregion TG*m* showed strong anatomical connections with the AMG, which could indicate its roles in emotional behavior in humans (Olson et al. 2007). Thirdly, reciprocal connections existed between the TP and the HIP in monkey studies (Moran et al. 1987). Here, the TG*m* and TG*l* demonstrated stronger probabilities with the HIP in both hemispheres, such that the connections with the HIP might be limited in the ventral TP. Finally, consistent with previous monkey studies of temporal corticostriate projections (Van Hoesen et al. 1981), we also observed anatomical connections between the TP subregions (particularly the TG*l* and TA*r*) with the PUT.

Limitations and Methodology Considerations

In this study, although the subregional organization and anatomical connections of the human TP were revealed in detail, the limitations of this study should also be emphasized. First, because of the inherent limitations of probabilistic tractography, fibers that run in parallel but belong to different tracts may be

difficult to distinguish, and the tracked fiber pathways may jump over and continue along a false tract. Thus, the IFOF observed in our study may be falsely reconstructed from the TP seeds, although it could be arbitrarily separated from the nearby fiber tracts using the JHU WM atlas. Furthermore, there are still debates concerning the presence of the IFOF among gross dissection (Curran 1909; Davis 1921) and DTI studies (Catani et al. 2002; O'Donnell et al. 2006) in the human brain. Schmahmann and Pandya (2006) and Schmahmann et al. (2007) have postulated that the apparent existence of an 'inferior FOF' as a continuous association fiber bundle may result from the conflation of the ILF caudally with the extreme capsule and/or UF rostrally. Secondly, given that there is signal dropout and stacking in the ventrolateral anterior temporal region behind the pole (Embleton et al. 2010). The worst of this problem is outside of the TP region, but it will affect the likely streamline paths and place limitations on the connectivity of the ventral aspects of the temporopolar cortex. Finally, with regard to the similarities and differences in the TP subregional functional and anatomical connectivity patterns, we thought that the anatomically connected subregions constituted a subset of the regions that were functionally connected. Previous studies have suggested that an RSFC analysis could detect meaningful anatomical connections and were not limited to anatomical connections in monkeys and humans (van den Heuvel et al. 2009). The RSFC mapped these brain areas and showed correlations in their activation, whereas those areas may or may not be directly interconnected. However, the anatomical connections among the brain regions revealed by diffusion data should be directly connected. Thus, in our findings, the traced fibers and anatomical connectivity fingerprints for the TP subregions could be a part of the functional connected networks.

Conclusions

To the best of our knowledge, this is the first study to parcel the human TP in vivo that is based on the anatomical connectivity features using DTI with probabilistic tractography. In terms of the TP subregional anatomical connection patterns, we could conclude that the underlying fiber pathways provide further evidence for the current parcellation in human TP and strongly suggest that the TP functioned as a transition zone to converge information from the frontal lobe, temporal lobe, and limbic system. Furthermore, the distinct functional and anatomical connectivity patterns of the TP subregions could support the diverse roles of the TP subregions in both multisensory integration and high-order cognitive functions. In conclusion, the parcellation framework and connectivity results may help to unravel the complex activation patterns in the TP from functional neuroimaging studies and may facilitate more detailed studies of this brain area in the future.

Supplementary Material

Supplementary material can be found at: http://www.cercor.oxfordjournals.org/.

Funding

This work was partially supported by the National Key Basic Research and Development Program (973) (grant no. 2011CB707801), the Strategic Priority Research Program of the Chinese Academy of Sciences (grant no. XDB02030300), and the Natural Science Foundation of China (grant no. 91132301).

Notes

The authors thank Dr Bing Hou and the anonymous reviewers offered constructive comments on the manuscript. *Conflict of Interest*: None declared.

References

Aggleton JP, Burton MJ, Passingham RE. 1980. Cortical and subcortical afferents to the amygdala of the rhesus monkey (*Macaca mulatta*). Brain Res. 190:347–368.
Aggleton JP, Mishkin M. 1984. Projections of the amygdala to the thalamus in the cynomolgus monkey. J Comp Neurol. 222:56–68.
Amaral DG, Price JL. 1984. Amygdalo-cortical projections in the monkey (*Macaca fascicularis*). J Comp Neurol. 230:465–496.
Arnold SE, Hyman BT, Van Hoesen GW. 1994. Neuropathologic changes of the temporal pole in Alzheimer's disease and Pick's disease. Arch Neurol. 51:145–150.
Averbeck BB, Battaglia-Mayer A, Guglielmo C, Caminiti R. 2009. Statistical analysis of parieto-frontal cognitive-motor networks. J Neurophysiol. 102:1911–1920.
Bach DR, Behrens TE, Garrido L, Weiskopf N, Dolan RJ. 2010. Deep and superficial amygdala nuclei projections revealed in vivo by probabilistic tractography. J Neurosci. 31:618–623.
Beckmann M, Johansen-Berg H, Rushworth MF. 2009. Connectivity-based parcellation of human cingulate cortex and its relation to functional specialization. J Neurosci. 29:1175–1190.
Behrens TE, Berg HJ, Jbabdi S, Rushworth MF, Woolrich MW. 2007. Probabilistic diffusion tractography with multiple fibre orientations: What can we gain? Neuroimage. 34:144–155.
Behrens TE, Johansen-Berg H, Woolrich MW, Smith SM, Wheeler-Kingshott CA, Boulby PA, Barker GJ, Sillery EL, Sheehan K, Ciccarelli O et al. 2003. Non-invasive mapping of connections between human thalamus and cortex using diffusion imaging. Nat Neurosci. 6:750–757.
Behrens TE, Woolrich MW, Jenkinson M, Johansen-Berg H, Nunes RG, Clare S, Matthews PM, Brady JM, Smith SM. 2003. Characterization and propagation of uncertainty in diffusion-weighted MR imaging. Magn Reson Med. 50:1077–1088.
Bi Y, Wei T, Wu C, Han Z, Jiang T, Caramazza A. 2010. The role of the left anterior temporal lobe in language processing revisited: evidence from an individual with ATL resection. Cortex. 47:575–587.
Binder JR, Desai RH, Graves WW, Conant LL. 2009. Where is the semantic system? A critical review and meta-analysis of 120 functional neuroimaging studies. Cereb Cortex. 19:2767–2796.
Binney RJ, Embleton KV, Jefferies E, Parker GJ, Ralph MA. 2010. The ventral and inferolateral aspects of the anterior temporal lobe are crucial in semantic memory: evidence from a novel direct comparison of distortion-corrected fMRI, rTMS, and semantic dementia. Cereb Cortex. 20:2728–2738.
Binney RJ, Parker GJ, Lambon Ralph MA. 2012. Convergent connectivity and graded specialization in the rostral human temporal lobe as revealed by diffusion-weighted imaging probabilistic tractography. J Cogn Neurosci. 24:1998–2014.
Biswal BB, Mennes M, Zuo XN, Gohel S, Kelly C, Smith SM, Beckmann CF, Adelstein JS, Buckner RL, Colcombe S et al. 2010. Toward discovery science of human brain function. Proc Natl Acad Sci USA. 107:4734–4739.
Blaizot X, Mansilla F, Insausti AM, Constans JM, Salinas-Alaman A, Pro-Sistiaga P, Mohedano-Moriano A, Insausti R. 2010. The human parahippocampal region: I. Temporal pole cytoarchitectonic and MRI correlation. Cereb Cortex. 20:2198–2212.
Brodmann K. 1909. Vergleichende Lokalisationslehre der Großhimrinde in ihren Prinzipien dargestellt auf Grund des Zellenbaues. Leipzig (Germany): Barth.

Buckner RL, Andrews-Hanna JR, Schacter DL. 2008. The brain's default network: anatomy, function, and relevance to disease. Ann N Y Acad Sci. 1124:1–38.
Caspers S, Eickhoff SB, Rick T, von Kapri A, Kuhlen T, Huang R, Shah NJ, Zilles K. 2011. Probabilistic fibre tract analysis of cytoarchitectonically defined human inferior parietal lobule areas reveals similarities to macaques. Neuroimage. 58:362–380.
Catani M, Howard RJ, Pajevic S, Jones DK. 2002. Virtual in vivo interactive dissection of white matter fasciculi in the human brain. Neuroimage. 17:77–94.
Catani M, Jones DK, Donato R, Ffytche DH. 2003. Occipito-temporal connections in the human brain. Brain. 126:2093–2107.
Chabardes S, Kahane P, Minotti L, Tassi L, Grand S, Hoffmann D, Benabid AL. 2005. The temporopolar cortex plays a pivotal role in temporal lobe seizures. Brain. 128:1818–1831.
Clarke S, Bellmann Thiran A, Maeder P, Adriani M, Vernet O, Regli L, Cuisenaire O, Thiran JP. 2002. What and where in human audition: selective deficits following focal hemispheric lesions. Exp Brain Res. 147:8–15.
Cloutman LL, Binney RJ, Drakesmith M, Parker GJ, Lambon Ralph MA. 2012. The variation of function across the human insula mirrors its patterns of structural connectivity: evidence from in vivo probabilistic tractography. Neuroimage. 59:3514–3521.
Cloutman LL, Lambon Ralph MA. 2012. Connectivity-based structural and functional parcellation of the human cortex using diffusion imaging and tractography. Front Neuroanat. 6:34.
Collins DL, Neelin P, Peters TM, Evans AC. 1994. Automatic 3D intersubject registration of MR volumetric data in standardized Talairach space. J Comput Assist Tomogr. 18:192–205.
Crespo-Facorro B, Nopoulos PC, Chemerinski E, Kim JJ, Andreasen NC, Magnotta V. 2004. Temporal pole morphology and psychopathology in males with schizophrenia. Psychiatry Res. 132:107–115.
Curran EJ. 1909. A new association fiber tract in the cerebrum with remarks on the fiber tract dissection method of studying the brain. J Comp Neurol Psychol. 19:645–656.
Davis LE. 1921. An anatomic study of the inferior longitudinal fasciculus. Arch Neurol Psychiatry. 5:370–381.
DeWitt I, Rauschecker JP. 2012. Phoneme and word recognition in the auditory ventral stream. Proc Natl Acad Sci USA. 109: E505–E514.
Ding SL, Van Hoesen GW, Cassell MD, Poremba A. 2009. Parcellation of human temporal polar cortex: a combined analysis of multiple cytoarchitectonic, chemoarchitectonic, and pathological markers. J Comp Neurol. 514:595–623.
Economo CV, Koskinas GN. 1925. Die Cytoarchitectonik der Hirnrinde des erwachsenen Menschen. Vienna, Berlin: Springer.
Eickhoff SB, Jbabdi S, Caspers S, Laird AR, Fox PT, Zilles K, Behrens TE. 2010. Anatomical and functional connectivity of cytoarchitectonic areas within the human parietal operculum. J Neurosci. 30:6409–6421.
Embleton KV, Haroon HA, Morris DM, Ralph MA, Parker GJ. 2010. Distortion correction for diffusion-weighted MRI tractography and fMRI in the temporal lobes. Hum Brain Mapp. 31:1570–1587.
Flechsig PE. 1920. Anatomie des menschlichen Gehirns and Rückenmarks auf myelogenetischer Grundlage. Thieme: Leipzig.
Fox MD, Snyder AZ, Vincent JL, Corbetta M, Van Essen DC, Raichle ME. 2005. The human brain is intrinsically organized into dynamic, anticorrelated functional networks. Proc Natl Acad Sci USA. 102:9673–9678.
Frith U, Frith C. 2010. The social brain: allowing humans to boldly go where no other species has been. Philos Trans R Soc B. 365:165–176.
Gloor P. 1997. The Temporal Lobe and Limbic System. USA: Oxford University Press.
Gower EC. 1989. Efferent projections from limbic cortex of the temporal pole to the magnocellular medial dorsal nucleus in the rhesus monkey. J Comp Neurol. 280:343–358.
Green S, Ralph MA, Moll J, Stamatakis EA, Grafman J, Zahn R. 2010. Selective functional integration between anterior temporal and distinct fronto-mesolimbic regions during guilt and indignation. Neuroimage. 52:1720–1726.
Gur RE, Turetsky BI, Cowell PE, Finkelman C, Maany V, Grossman RI, Arnold SE, Bilker WB, Gur RC. 2000. Temporolimbic volume reductions in schizophrenia. Arch Gen Psychiatry. 57:769–775.
Hickok G, Poeppel D. 2007. The cortical organization of speech processing. Nat Rev Neurosci. 8:393–402.
Holland R, Lambon Ralph MA. 2010. The anterior temporal lobe semantic hub is a part of the language neural network: selective disruption of irregular past tense verbs by rTMS. Cereb Cortex. 20:2771–2775.
Hopf A. 1954. Die Myeloarchitektonik des Isokortex temporalis beim Menschen. J Hirnforschung 1:208–279.
Insausti R, Juottonen K, Soininen H, Insausti AM, Partanen K, Vainio P, Laakso MP, Pitkanen A. 1998. MR volumetric analysis of the human entorhinal, perirhinal, and temporopolar cortices. AJNR Am J Neuroradiol. 19:659–671.
Johansen-Berg H, Behrens TE, Robson MD, Drobnjak I, Rushworth MF, Brady JM, Smith SM, Higham DJ, Matthews PM. 2004. Changes in connectivity profiles define functionally distinct regions in human medial frontal cortex. Proc Natl Acad Sci USA. 101:13335–13340.
Kahnt T, Chang LJ, Park SQ, Heinzle J, Haynes JD. 2012. Connectivity-based parcellation of the human orbitofrontal cortex. J Neurosci. 32:6240–6250.
Klingler J, Gloor P. 1960. The connections of the amygdala and of the anterior temporal cortex in the human brain. J Comp Neurol. 115:333–369.
Kondo H, Saleem KS, Price JL. 2003. Differential connections of the temporal pole with the orbital and medial prefrontal networks in macaque monkeys. J Comp Neurol. 465:499–523.
Kucyi A, Moayedi M, Weissman-Fogel I, Hodaie M, Davis KD. 2012. Hemispheric asymmetry in white matter connectivity of the temporoparietal junction with the insula and prefrontal cortex. PLoS One. 7:e35589.
Lavenex P, Amaral DG. 2000. Hippocampal-neocortical interaction: a hierarchy of associativity. Hippocampus. 10:420–430.
Makris N, Papadimitriou GM, Kaiser JR, Sorg S, Kennedy DN, Pandya DN. 2009. Delineation of the middle longitudinal fascicle in humans: a quantitative, in vivo, DT-MRI study. Cereb Cortex. 19:777–785.
Markowitsch HJ, Emmans D, Irle E, Streicher M, Preilowski B. 1985. Cortical and subcortical afferent connections of the primate's temporal pole: a study of rhesus monkeys, squirrel monkeys, and marmosets. J Comp Neurol. 242:425–458.
Mars RB, Jbabdi S, Sallet J, O'Reilly JX, Croxson PL, Olivier E, Noonan MP, Bergmann C, Mitchell AS, Baxter MG et al. 2011. Diffusion-weighted imaging tractography-based parcellation of the human parietal cortex and comparison with human and macaque resting-state functional connectivity. J Neurosci. 31:4087–4100.
Mars RB, Sallet J, Schuffelgen U, Jbabdi S, Toni I, Rushworth MF. 2011. Connectivity-based subdivisions of the human right "temporoparietal junction area": evidence for different areas participating in different cortical networks. Cereb Cortex. 22:1894–1903.
Mesulam MM, Mufson EJ. 1982. Insula of the old world monkey. I. Architectonics in the insulo-orbito-temporal component of the paralimbic brain. J Comp Neurol. 212:1–22.
Moran MA, Mufson EJ, Mesulam MM. 1987. Neural inputs into the temporopolar cortex of the rhesus monkey. J Comp Neurol. 256:88–103.
Morecraft RJ, Geula C, Mesulam MM. 1992. Cytoarchitecture and neural afferents of orbitofrontal cortex in the brain of the monkey. J Comp Neurol. 323:341–358.
Mufson EJ, Mesulam MM. 1982. Insula of the old world monkey. II: afferent cortical input and comments on the claustrum. J Comp Neurol. 212:23–37.
Mummery CJ, Patterson K, Wise RJ, Vandenberghe R, Price CJ, Hodges JR. 1999. Disrupted temporal lobe connections in semantic dementia. Brain. 122(Pt 1):61–73.
Munoz M, Insausti R. 2005. Cortical efferents of the entorhinal cortex and the adjacent parahippocampal region in the monkey (*Macaca fascicularis*). Eur J Neurosci. 22:1368–1388.

Munoz-Lopez MM, Mohedano-Moriano A, Insausti R. 2010. Anatomical pathways for auditory memory in primates. Front Neuroanat. 4:129.
Murphy K, Bodurka J, Bandettini PA. 2007. How long to scan? The relationship between fMRI temporal signal to noise ratio and necessary scan duration. Neuroimage. 34:565–574.
Nakamura K, Kawashima R, Sato N, Nakamura A, Sugiura M, Kato T, Hatano K, Ito K, Fukuda H, Schormann T et al. 2000. Functional delineation of the human occipito-temporal areas related to face and scene processing. A PET study. Brain. 123(Pt 9):1903–1912.
Nakamura K, Kubota K. 1996. The primate temporal pole: its putative role in object recognition and memory. Behav Brain Res. 77:53–77.
Nakamura K, Matsumoto K, Mikami A, Kubota K. 1994. Visual response properties of single neurons in the temporal pole of behaving monkeys. J Neurophysiol. 71:1206–1221.
Nauta WJ. 1961. Fibre degeneration following lesions of the amygdaloid complex in the monkey. J Anat. 95:515–531.
Ng AY, Jordan MI, Weiss Y. 2002. On spectral clustering: analysis and an algorithm. Adv Neural Inf Process Systems. 14:849–856.
O'Donnell LJ, Kubicki M, Shenton ME, Dreusicke MH, Grimson WE, Westin CF. 2006. A method for clustering white matter fiber tracts. AJNR Am J Neuroradiol. 27:1032–1036.
Olson IR, McCoy D, Klobusicky E, Ross LA. 2012. Social cognition and the anterior temporal lobes: a review and theoretical framework. Soc Cogn Affect Neurosci. 8:123–133.
Olson IR, Plotzker A, Ezzyat Y. 2007. The enigmatic temporal pole: a review of findings on social and emotional processing. Brain. 130:1718–1731.
Pandya DN, Kuypers HG. 1969. Cortico-cortical connections in the rhesus monkey. Brain Res. 13:13–36.
Passingham RE, Stephan KE, Kotter R. 2002. The anatomical basis of functional localization in the cortex. Nat Rev Neurosci. 3:606–616.
Patterson K, Nestor PJ, Rogers TT. 2007. Where do you know what you know? The representation of semantic knowledge in the human brain. Nat Rev Neurosci. 8:976–987.
Petrides M, Pandya DN. 1988. Association fiber pathways to the frontal cortex from the superior temporal region in the rhesus monkey. J Comp Neurol. 273:52–66.
Petrides M, Pandya DN. 2002. Comparative cytoarchitectonic analysis of the human and the macaque ventrolateral prefrontal cortex and corticocortical connection patterns in the monkey. Eur J Neurosci. 16:291–310.
Petrides M, Pandya DN. 2009. Distinct parietal and temporal pathways to the homologues of Broca's area in the monkey. PLoS Biol. 7: e1000170.
Pobric G, Jefferies E, Ralph MA. 2007. Anterior temporal lobes mediate semantic representation: mimicking semantic dementia by using rTMS in normal participants. Proc Natl Acad Sci USA. 104:20137–20141.
Poremba A, Malloy M, Saunders RC, Carson RE, Herscovitch P, Mishkin M. 2004. Species-specific calls evoke asymmetric activity in the monkey's temporal poles. Nature. 427:448–451.
Poremba A, Saunders RC, Crane AM, Cook M, Sokoloff L, Mishkin M. 2003. Functional mapping of the primate auditory system. Science. 299:568–572.
Rankin KP, Gorno-Tempini ML, Allison SC, Stanley CM, Glenn S, Weiner MW, Miller BL. 2006. Structural anatomy of empathy in neurodegenerative disease. Brain. 129:2945–2956.
Rauschecker JP, Scott SK. 2009. Maps and streams in the auditory cortex: nonhuman primates illuminate human speech processing. Nat Neurosci. 12:718–724.
Royet JP, Zald D, Versace R, Costes N, Lavenne F, Koenig O, Gervais R. 2000. Emotional responses to pleasant and unpleasant olfactory, visual, and auditory stimuli: a positron emission tomography study. J Neurosci. 20:7752–7759.
Saleem KS, Suzuki W, Tanaka K, Hashikawa T. 2000. Connections between anterior inferotemporal cortex and superior temporal sulcus regions in the macaque monkey. J Neurosci. 20:5083–5101.
Schacter DL, Wagner AD. 1999. Medial temporal lobe activations in fMRI and PET studies of episodic encoding and retrieval. Hippocampus. 9:7–24.
Schmahmann JD, Pandya DN. 2006. Fiber pathways of the brain. New York: Oxford University Press.
Schmahmann JD, Pandya DN, Wang R, Dai G, D'Arceuil HE, de Crespigny AJ, Wedeen VJ. 2007. Association fibre pathways of the brain: parallel observations from diffusion spectrum imaging and autoradiography. Brain. 130:630–653.
Scott SK, Blank CC, Rosen S, Wise RJ. 2000. Identification of a pathway for intelligible speech in the left temporal lobe. Brain. 123(Pt 12):2400–2406.
Semah F. 2002. Temporoporal metabolic abnormalities in temporal lobe epilepsies. Epileptic Disord. 4(Suppl 1):S41–S49.
Sewards TV. 2011. Adolf Hopf's 1954 myeloarchitectonic parcellation of the human temporal lobe: a review and assessment. Brain Res Bull. 86:298–313.
Simmons WK, Reddish M, Bellgowan PS, Martin A. 2010. The selectivity and functional connectivity of the anterior temporal lobes. Cereb Cortex. 20:813–825.
Skipper LM, Ross LA, Olson IR. 2011. Sensory and semantic category subdivisions within the anterior temporal lobes. Neuropsychologia. 49:3419–3429.
Sled JG, Zijdenbos AP, Evans AC. 1998. A nonparametric method for automatic correction of intensity nonuniformity in MRI data. IEEE Trans Med Imaging. 17:87–97.
Smith SM. 2002. Fast robust automated brain extraction. Hum Brain Mapp. 17:143–155.
Stefanacci L, Suzuki WA, Amaral DG. 1996. Organization of connections between the amygdaloid complex and the perirhinal and parahippocampal cortices in macaque monkeys. J Comp Neurol. 375:552–582.
Tomassini V, Jbabdi S, Klein JC, Behrens TE, Pozzilli C, Matthews PM, Rushworth MF, Johansen-Berg H. 2007. Diffusion-weighted imaging tractography-based parcellation of the human lateral premotor cortex identifies dorsal and ventral subregions with anatomical and functional specializations. J Neurosci. 27:10259–10269.
Tzourio-Mazoyer N, Landeau B, Papathanassiou D, Crivello F, Etard O, Delcroix N, Mazoyer B, Joliot M. 2002. Automated anatomical labeling of activations in SPM using a macroscopic anatomical parcellation of the MNI MRI single-subject brain. Neuroimage. 15:273–289.
Ueno T, Saito S, Rogers TT, Lambon Ralph MA. 2011. Lichtheim 2: synthesizing aphasia and the neural basis of language in a neurocomputational model of the dual dorsal-ventral language pathways. Neuron. 72:385–396.
van den Heuvel MP, Mandl RC, Kahn RS, Hulshoff Pol HE. 2009. Functionally linked resting-state networks reflect the underlying structural connectivity architecture of the human brain. Hum Brain Mapp. 30:3127–3141.
Van Essen DC, Glasser MF, Dierker DL, Harwell J, Coalson T. 2012. Parcellations and hemispheric asymmetries of human cerebral cortex analyzed on surface-based atlases. Cereb Cortex. 22: 2241–2262.
Van Hoesen GW, Yeterian EH, Lavizzo-Mourey R. 1981. Widespread corticostriate projections from temporal cortex of the rhesus monkey. J Comp Neurol. 199:205–219.
Visser M, Jefferies E, Embleton KV, Lambon Ralph MA. 2012. Both the middle temporal gyrus and the ventral anterior temporal area are crucial for multimodal semantic processing: distortion-corrected fMRI evidence for a double gradient of information convergence in the temporal lobes. J Cogn Neurosci. 24:1766–1778.
Visser M, Jefferies E, Lambon Ralph MA. 2010. Semantic processing in the anterior temporal lobes: a meta-analysis of the functional neuroimaging literature. J Cogn Neurosci. 22:1083–1094.
Visser M, Lambon Ralph MA. 2011. Differential contributions of bilateral ventral anterior temporal lobe and left anterior superior temporal gyrus to semantic processes. J Cogn Neurosci. 23:3121–3131.
Wakana S, Jiang H, Nagae-Poetscher LM, van Zijl PC, Mori S. 2004. Fiber tract-based atlas of human white matter anatomy. Radiology. 230:77–87.

Wang J, Fan L, Zhang Y, Liu Y, Jiang D, Yu C, Jiang T. 2012. Tractography-based parcellation of the human left inferior parietal lobule. Neuroimage. 63:641–652.
Wang Y, Fernandez-Miranda JC, Verstynen T, Pathak S, Schneider W, Yeh FC. 2013. Rethinking the role of the middle longitudinal fascicle in language and auditory pathways. Cereb Cortex. 23: 2347–2356.
Wirth M, Jann K, Dierks T, Federspiel A, Wiest R, Horn H. 2011. Semantic memory involvement in the default mode network: a functional neuroimaging study using independent component analysis. Neuroimage. 54:3057–3066.
Zahn R, Moll J, Krueger F, Huey ED, Garrido G, Grafman J. 2007. Social concepts are represented in the superior anterior temporal cortex. Proc Natl Acad Sci USA. 104:6430–6435.
Zahn R, Moll J, Paiva M, Garrido G, Krueger F, Huey ED, Grafman J. 2009. The neural basis of human social values: evidence from functional MRI. Cereb Cortex. 19: 276–283.